Society for
Mathematical
Biology

Check for
updates

Age Structure Can Account for Delayed Logistic Proliferation of Scratch Assays

Ana Victoria Ponce Bobadilla[1,2] (iD) · **Thomas Carraro**[1,2] (iD) · **Helen M. Byrne**[3] (iD) ·
Philip K. Maini[3] (iD) · **Tomás Alarcón**[4,5,6,7] (iD)

Abstract

Scratch assays are in vitro methods for studying cell migration. In these experiments, a scratch is made on a cell monolayer and recolonisation of the scratched region is imaged to quantify cell migration rates. Typically, scratch assays are modelled by reaction diffusion equations depicting cell migration by Fickian diffusion and proliferation by a logistic term. In a recent paper (Jin et al. in Bull Math Biol 79(5):1028–1050, 2017), the authors observed experimentally that during the early stage of the recolonisation process, there is a disturbance phase where proliferation is not logistic, and this is followed by a growth phase where proliferation appears to be logistic. The authors did not identify the precise mechanism that causes the disturbance phase but showed that ignoring it can lead to incorrect parameter estimates. The aim of this work is to show that a nonlinear age-structured population model can account for the two phases of proliferation in scratch assays. The model consists of an age-structured cell cycle model of a cell population, coupled with an ordinary differential equation describing the resource concentration dynamics in the substrate. The model assumes a resource-dependent cell cycle threshold age, above which cells are able to proliferate. By studying the dynamics of the full system in terms of the subpopulations of cells that can proliferate and the ones that can not, we are able to find conditions under which the model captures the two-phase behaviour. Through numerical simulations, we are able to show that the interplay between the resource concentration in the substrate and the cell subpopulations dynamics can explain the biphasic dynamics.

✉ Ana Victoria Ponce Bobadilla
   anavictoria.ponce@iwr.uni-heidelberg.de

Extended author information available on the last page of the article

Springer

1 Introduction

Cell migration and proliferation are central processes in the development and homoeostasis of many organisms. They also play a key role in pathological processes such as cancer invasion, chronic inflammatory diseases and vascular diseases (Cohen and Ellwein 1990; Liu et al. 2017; Menyhárt et al. 2016). To understand the biochemical and physical cues that regulate cell migration and proliferation, in vitro assays are used to quantify the ability of cell populations to migrate and proliferate under controlled situations (Adan et al. 2016; Celis 2009; Kramer et al. 2013). Scratch assays are typically used to study cell migration (Kramer et al. 2013; Liang et al. 2007). A scratch assay involves: growing a cell monolayer to confluence; creating a "scratch" in the monolayer; and monitoring the cell dynamics as the scratch closes (Liang et al. 2007). The resulting time-course data are then analysed to estimate the cell migration rate (Masuzzo et al. 2016; Topman et al. 2012). Other common cell-based assays are proliferation assays that focus on measuring the cell number or the proportion of cells that are dividing (Romar et al. 2016). The simplest proliferation assay consists of growing a cell monolayer to low density on a two-dimensional substrate and measuring the cell number change in time (Bourseguin et al. 2016; Browning et al. 2017; Romar et al. 2016). See Fig. 1a, b for a schematic representation of the typical time progression of these two in vitro assays.

Many mathematical models have been developed to describe these in-vitro assays and to test hypotheses concerning the mechanisms that govern cell migration and proliferation (Billy et al. 2012; Gerlee 2013; Jin et al. 2016; Johnston et al. 2015; Kramer et al. 2013; Maini et al. 2004; Nardini and Bortz 2018; Savla et al. 2004; Walker et al. 2004a, b). The macroscale dynamics of scratch assays are often described by reaction-diffusion equations (Jin et al. 2016; Maini et al. 2004; Savla et al. 2004) in which cell migration is modelled as Fickian diffusion and cell proliferation is modelled by a logistic source term. For the proliferation assay, where no scratch is performed, the logistic growth equation is widely used (Gerlee 2013; Johnston et al. 2015; Kramer et al. 2013). Models are calibrated by fitting their solutions to the experimental time-course data. A model is considered valid if the residual error is below a prescribed value (Jin et al. 2017; Sarapata and de Pillis 2014; West et al. 2001). However, as several authors have remarked, this condition may not be sufficient for model validation (Baker and Simpson 2010; Warne et al. 2018).

In Jin et al. (2017), the ability of the logistic growth model to describe cell proliferation in scratch assays was studied. A series of scratch and proliferation assays using PC-3 prostate cancer cells were performed, and the changes in cell density in two subregions located far from the scratch were quantified. These two subregions were chosen so the changes in cell density were not due to cell migration. To assess the suitability of the logistic growth model, they analysed the model fit to experimental data and the per capita growth rate of the experimental data, $\sigma(N) = \frac{dN}{dt} \frac{1}{N}$, as a function of the cell density, N. Calibrating solutions of the logistic model to the experimental
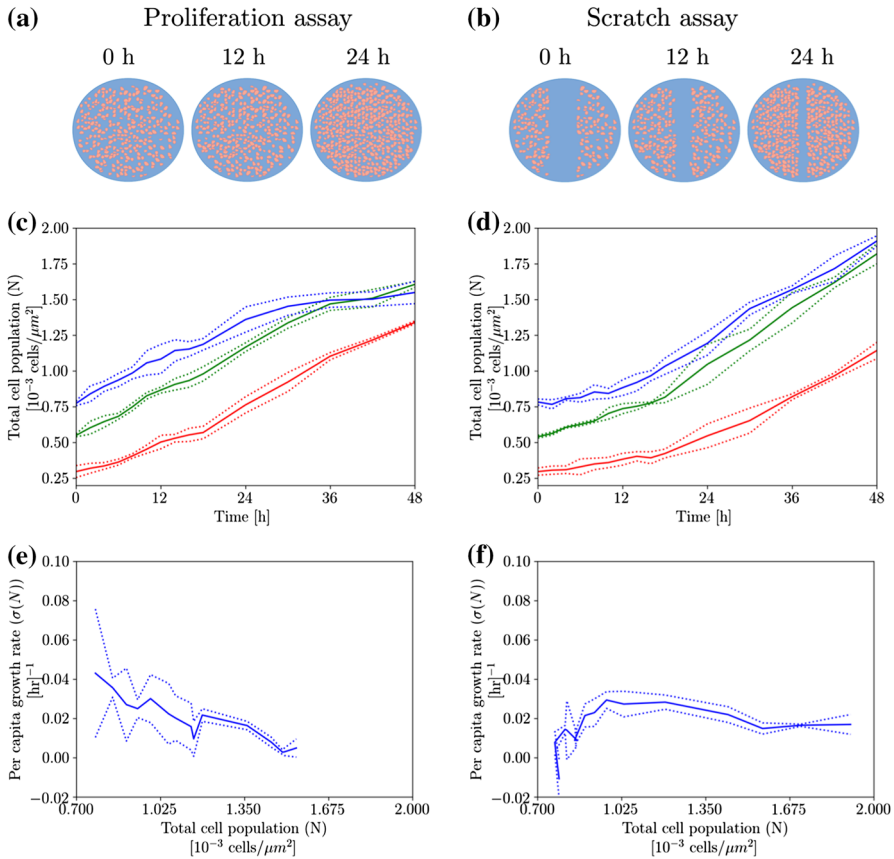
Fig. 1 Schematic representation of how the **a** proliferation and **b** scratch assays evolve in time. In the plots **c–f**, we consider the experimental data from the proliferation and scratch assays performed in Jin et al. (2017). The authors consider three replicates for three initial degrees of confluence. In **c** and **d**, the mean and the standard deviation of the cell population are plotted for each initial degree of confluence. In **e** and **f**, the mean and the standard deviation of the per capita growth rate $\sigma(N) = \frac{dN}{dt}\frac{1}{N}$ are plotted with respect to the mean cell population N. For plots **e** and **f**, we consider only the assays with the highest degree of confluence. We calculate the per capita growth rate in the same way as in Jin et al. (2017). A biphasic trend can be observed in **f** (for the scratch assay) but not in **e** (for the proliferation assay) (Colour figure online)

data showed a good fit for both assays; however, analysing the per capita growth rate revealed different behaviours between the proliferation and the scratch assays. The authors observed that for proliferation assays, the per capita growth rate could be well described by a linearly decreasing function of the cell density (see Fig. 1e), a result consistent with the logistic model. However, for the scratch assay data, during the first 18 h of the experiment, the per capita growth rate was found to increase with cell density, whereas for $8 \leq t \leq 48$ h, the per capita growth rate was found to decrease approximately linearly with the cell density (see Fig. 1f).

Guided by their experimental observations, the authors in Jin et al. (2017) proposed that cell proliferation in scratch assays involves two phases: an initial *disturbance*

phase during which proliferation is not logistic and a *growth phase* during which proliferation is approximately logistic. Since this behaviour was not observed in the proliferation assays, the authors concluded that it was caused by the scratching procedure. They hypothesised that scratching might create chemical or mechanical disturbances but did not test their hypothesis.

In this work, we show that a nonlinear age-structured model can account for the disturbance and growth phases observed in scratch assays. We refer to a cell's *age* as the cell's temporal position within the cell cycle. The cell cycle consists of four phases: first gap G_1, synthesis stage S, second gap G_2 and mitosis stage M. G_1 and G_2 consist of growth phases, DNA replication occurs in S phase and cell division in M phase (Darnell et al. 1990). The progression in the cell cycle is regulated by environmental cues and intracellular checkpoints involving various proteins, in particular cyclins and cyclin-dependent kinases (Darnell et al. 1990; Lim and Kaldis 2013).

By considering an age-structured model, we can investigate how heterogeneity in the cell population age distribution affects the total cell population dynamics. Previous work has shown that heterogeneity in cell age distribution may still generate logistic growth at the population scale (Jin et al. 2018). Other age-structured models have described how the cell age distribution can affect the overall cell population dynamics in scratch assays: the speed with which the cells invade the vacant region (Gavagnin et al. 2018; Vittadello et al. 2018), the efficacy of anti-cancer drugs, particularly phase-specific drugs (Billy and Clairambault 2013) and the influence of growth factors (Billy et al. 2012). Agent-based models have also been considered to study the effect of heterogeneity in cell age distribution on the overall dynamics in in vitro assays (Walker et al. 2004a, b).

We consider an age-structured model that was first introduced in de la Cruz et al. (2016). The model considers the interplay between a single cell population and the resource concentration available in the substrate. The model assumes a resource-dependent $G1/S$ transition age above which cells are able to proliferate. This critical age naturally divides the cell population into "immature" and "mature" cells. By studying the dynamics of the full system in terms of these subpopulations, we are able to find conditions under which the cell population evolution is of logistic-type and the per capita growth rate follows a biphasic behaviour. We validate our predictions via numerical simulations and show that the resource concentration regulates the disturbance phase.

The remainder of this paper is organised as follows. In Sect. 2, we describe the nonlinear age-structured model. In Sect. 3, we describe the dynamics of the full model in terms of the mature and immature subpopulation dynamics. We then derive conditions under which the per capita growth rate will exhibit biphasic behaviour and logistic-type proliferation. In Sect. 4, we investigate numerically these conditions and determine parameter regimes in which the resource concentration regulates the disturbance phase. We conclude in Sect. 5 with a discussion of the results and conclusions.

2 An Age-Structured Model with Resource-Regulated Proliferation

To take into account the cell cycle heterogeneity of a cell population, we consider a McKendrick–von Foerster model (Kermack and McKendrick 1932; Keyfitz and Keyfitz 1997). The model considered in this work was first used to describe the mean field dynamics of a stochastic multiscale model of a cell population with oxygen-regulated proliferation (de la Cruz et al. 2016). Here, the model describes the dynamics of an in vitro cell population assumed homogeneously distributed in space, like cell cultures in proliferation assays or cells in far away regions from the wound in scratch assays, as in Jin et al. (2017). We are interested in the population dynamics with respect to the resources available in the medium. We denote by $n(a, t)$, the number of cells of age a at time t. We consider $a \in [0, \infty]$. We denote by $T > 0$ the duration of the experimental observation. The model focuses on the cell population proliferation dependence on the growth factors, oxygen and nutrients available in the medium. We refer to these components as a single, generic *resource* and denote it by $c(t)$.

We assume cells mature with constant speed 1, die with rate μ and proliferate at a rate $b(a, c(t))$ which we consider to be age and resource-dependent (Ortmann et al. 2014; Smith et al. 1984). Combining the above assumptions, it is straightforward to show that the evolution of the cell density function $n(a, t) : [0, \infty] \times [0, T] \to \mathbb{R}$ is therefore given by

$$\frac{\partial n(a, t)}{\partial t} + \frac{\partial n(a, t)}{\partial a} = -(\mu + b(a, c(t)))n(a, t). \tag{1}$$

We suppose further that when a cell divides it produces two daughter cells of age $a = 0$. By considering all possible division events, we deduce that

$$n(0, t) = 2 \int_0^\infty b(a, c(t))n(a, t)\mathrm{d}a. \tag{2}$$

We consider a coarse-grained description of the cell cycle by lumping S, $G2$ and M into one phase, so we consider a two-phase model $G1$ and S–$G2$–M. We assume cells proliferate at a constant rate, τ_p^{-1}, provided they successfully enter the S–$G2$–M phase. Entry to the S–$G2$–M phase is regulated by the $G1/S$ checkpoint which has been shown to depend on the presence of resources needed for cell growth (Foster et al. 2010). Therefore, we assume that the proliferation rate is given by

$$b(a, c(t)) := \tau_p^{-1} H(a - a_{G1/S}(c(t))) \tag{3}$$

where H is the Heaviside function and $a_{G1/S}(c(t))$ denotes *the G1/S transition age*, the age at which a cell passes from the G1 to the S phase.

The $G1/S$ transition age, $a_{G1/S}(c)$ is given as a function of c to capture the dependence of the checkpoint on the available resource concentration. The authors in de la Cruz et al. (2016) describe this dependence by a simple scaling which was derived from analysing an oxygen-dependent cell cycle progression model,

$$a_{G1/S}(c) = \begin{cases} a_- \left(\frac{c}{c_{cr}} - 1 \right)^{-\beta} & \text{for } c > c_{cr}, \\ \infty & \text{for } c \leq c_{cr}, \end{cases}$$

where a_- and β are positive constants. The positive quantity c_{cr} is the critical resource concentration that allows cell proliferation. For high resource values, the transition age becomes smaller, so the cell requires less time to proliferate. On the other hand, for resource values slightly higher than c_{cr}, the transition age becomes bigger and cells take longer to transition to the $G1/S$ phase and to proliferate. For $c \leq c_{cr}$, cells are assumed to enter the quiescent state.

If we assume that the resource, $c(t)$, is supplied at a constant rate $\overline{S}$ and consumed by all cells at a constant rate k, then

$$\frac{dc}{dt} = \overline{S} - kNc, \tag{4}$$

where $N(t) = \int_0^\infty n(a, t)da$ denotes the total number of cells at time t.

The full model consists of Eqs. (1)–(4) and the initial conditions

$$n(a, 0) = v_0(a) \text{ for } a > 0 \text{ and } c(0) = c_0 \text{ where } c_0 > 0. \tag{5}$$

The long-time dynamics of this model was described in de la Cruz et al. (2016). Before beginning our analysis, we summarise below those results from de la Cruz et al. (2016) that are relevant for our work.

- For large times, the solution of the age-structured model approaches a separable solution, $Q(a, t) = A(a) \exp(\lambda t)$, i.e. $n(a, t) \approx Q(a, t)$ for $t \gg 1$, where λ satisfies the *Euler–Lotka equation*:

$$1 = 2 \int_0^\infty b(a, c_\infty) \exp \left(-\lambda a - \int_0^a [\mu + b(y, c_\infty)] \, dy \right) da \tag{6}$$

in which $c_\infty > 0$ is the steady-state value of the resource concentration. $A(a)$ is referred to as the *stable age distribution* of the model. The separable solution is assumed to be in equilibrium when $\lambda = 0$ and therefore $N(t) \to N_\infty$ and $\frac{dN}{dt} \to 0$ as $t \to \infty$.

- For the separable solution to be in equilibrium, the average waiting time to division after the $G1/S$ transition, τ_p, must be smaller than the average cell life span, μ^{-1}.

$$\tau_p < \mu^{-1}. \tag{7}$$

- If Eq. (7) is satisfied, after solving Eq. (6) with $\lambda = 0$, they obtained that:

  – The transition age, $a_{G1/S}$, reaches the steady-state value

$$a^* = -\frac{1}{\mu} \log \left(\frac{\tau_p(\mu + \tau_p^{-1})}{2} \right). \tag{8}$$

– The steady-state resource concentration is given by

$$c_\infty = a_{G1/S}^{-1}\left(a^*\right). \tag{9}$$

– The steady-state value of the total cell population density is given by:

$$N_\infty = \frac{\overline{S}}{kc_\infty}. \tag{10}$$

The above results will be useful for parametrising our model.

3 Model Analysis

In this section, we derive necessary and sufficient conditions for Eqs. (1)–(5) to exhibit logistic-type behaviour and biphasic behaviour in the per capita growth rate.

These conditions can be obtained by distinguishing two subpopulations: cells whose age is greater than the $G1/S$ transition age and which can proliferate, and cells whose age is below the threshold. We refer to these subpopulations as, respectively, *mature* and *immature* cells. We now analyse the full system with respect to these subpopulation dynamics.

3.1 Mature and Immature Subpopulation Dynamics

Let us denote by $X(t)$ and $Y(t)$, respectively, the subpopulations of mature and immature cells so that

$$X(t) = \int_0^{a_{G1/S}(t)} n(a,t)\mathrm{d}a \quad\text{and}\quad Y(t) = \int_{a_{G1/S}(t)}^\infty n(a,t)\mathrm{d}a, \tag{11}$$

where $a_{G1/S}(t) := a_{G1/S}(c(t))$.

With these definitions, it is possible to obtain the following result:

Theorem 1 *Let X and Y be defined as in (11) and let $n(a,t)$ and $c(t)$ satisfy the model Eqs. (1)–(5). Then, the dynamics of X and Y are given by the following system:*

$$\frac{\mathrm{d}X}{\mathrm{d}t} = 2\tau_p^{-1}Y - \mu X + \left[\frac{\mathrm{d}a_{G1/S}}{\mathrm{d}t}(t) - 1\right]n(a_{G1/S}(t),t),$$

$$\frac{\mathrm{d}Y}{\mathrm{d}t} = -(\mu + \tau_p^{-1})Y + \left[1 - \frac{\mathrm{d}a_{G1/S}}{\mathrm{d}t}(t)\right]n(a_{G1/S}(t),t), \tag{12}$$

in which $a_{G1/S}(t) := a_-\left(\frac{c(t)}{c_{\mathrm{cr}}} - 1\right)^{-\beta}$ and $c(t)$ is formally given by

$$c(t) = \left[c_0 + \overline{S}\int_0^t \exp\left(k\int_0^{t'} N(s)\mathrm{d}s\right)\mathrm{d}t'\right]\exp\left(-k\int_0^t N(s)\mathrm{d}s\right).$$

Furthermore, if $c(t) \geq c_{cr} \; \forall t \in [0, T]$, then the number of cells with $G1/S$ transition age $a_{G1/S}(t)$ at time t, $n(a_{G1/S}(t), t)$, is formally given by

$$n(a_{G1/S}(t), t) = v_0(a_{G1/S}(t) - t) \exp\left(-\int_0^t [\mu + b(s - t + a_{G1/S}(t), c(s))]ds\right)$$
(13)

for $t \leq a_{G1/S}(t)$ and

$$n(a_{G1/S}(t), t)$$
$$= 2\tau_p^{-1} Y(t - a_{G1/S}(t)) \exp\left(-\int_0^{a_{G1/S}(t)} [\mu + b(s, c(s + t - a_{G1/S}(t)))]ds\right)$$
(14)

for $t > a_{G1/S}(t)$.

Proof

Integrating Eq. (1) over the domains $[0, a_{G1/S}(t)]$ and $[a_{G1/S}(t), \infty]$, we obtain the dynamics of X and Y, respectively. The evolution of $c(t)$ is given by solving the differential Eq. (4), while assuming $N(t)$ is a known function. Finally, the formula for the cell concentration with $G1/S$ transition age $a_{G1/S}(t)$ at time t, $n(a_{G1/S}(t), t)$, is obtained by solving the age-structured model by the method of characteristics. The characteristic curves of Eq. (1) are the lines $a = t + \mu$ where μ is a constant. By solving Eq. (1) along the characteristic curves and taking into account the boundary condition (2) and initial condition (5), we obtain that $n(a, t)$ is given by:

$$n(a, t) = \begin{cases} v_0(a - t) \exp\left(-\int_0^t [\mu + b(s - t + a, c(s))]ds\right) & \text{for } t \leq a, \\ n(0, t - a) \exp\left(-\int_0^a [\mu + b(s, c(s + t - a))]ds\right) & \text{for } a < t. \end{cases}$$
(15)

By considering $a = a_{G1/S}(t)$ and $n(0, t - a_{G1/S}(t))$ in terms of the mature subpopulation Y in Eq. (15), we derive expressions (13) and (14) for $n(a_{G1/S}(t), t)$. $\qquad \square$

Theorem 1 reduces the analysis of the full model to the analysis of system (12). Given Eqs. (13) and (14), we notice that for $t \leq a_{G1/S}(t)$, (12) consists of a non-homogeneous coupled linear system of ordinary differential equations that depends on the initial age distribution and for $t > a_{G1/S}(t)$, the dynamics of Y is described by a state-dependent delay differential equation,

$$\frac{dY}{dt} = -(\mu + \tau_p^{-1})Y + 2\tau_p^{-1} \overline{a}(t) Y(t - a_{G1/S}(t))$$
(16)

in which $\overline{a}(t) = \left[1 - a'_{G1/S}(t)\right] \exp\left(-\int_0^{a_{G1/S}(t)} [\mu + b(s, c(s + t - a))]ds\right)$.

Having the dynamics of the full model expressed in terms of these subpopulations, we can now describe the overall proliferation and the per capita growth rate in terms of the dynamics of these two subpopulations. Let us denote by $\sigma(N(t)) := \frac{dN(t)}{dt} \frac{1}{N(t)}$, the per capita growth rate. The following theorem gives the evolution of the per capita

growth rate and the total population evolution in terms of the mature and immature cell subpopulations.

Theorem 2 *The evolution of $N(t)$ and $\sigma(N(t))$ for $t \in [0, T]$ is given by:*

$$\frac{dN}{dt} = [\tau_p^{-1} - \mu]Y - \mu X, \tag{17}$$

$$\frac{d\sigma(N(t))}{dt} = \tau_p^{-1} \frac{d}{dt}\left[\frac{Y}{N}\right]. \tag{18}$$

Proof By integrating Eq. (1) in the age domain $[0, \infty]$, we obtain Eq. (17). To derive Eq. (18), we consider the definition of the per capita growth rate and Eq. (17) as follows,

$$\frac{d\sigma(N(t))}{dt} = \frac{d}{dt}\left[\frac{\frac{dN}{dt}}{N}\right] = \frac{d}{dt}\left[\frac{(\tau_p^{-1} - \mu)Y - \mu X}{N}\right]$$
$$= \frac{d}{dt}\left[\tau_p^{-1}\frac{Y}{N} - \mu\right] = \tau_p^{-1}\frac{d}{dt}\left[\frac{Y}{N}\right]$$

from which we obtain Eq. (18).   □

3.2 Conditions for Delayed Logistic Proliferation

In this section, we identify conditions under which the per capita growth rate of the age-structured model exhibits biphasic dynamics and logistic-type growth. First, we interpret the experimental behaviour in mathematical terms:

B1 The cell population undergoes a logistic-type behaviour, i.e.

  • The population increases in size monotonically,

$$\frac{dN}{dt} > 0 \qquad \forall t \in [0, T].$$

  • The population saturates

$$N(t) \to N_\infty. \quad \text{as} \quad t \to T,$$

  where $N_\infty > 0$.

B2 The per capita growth rate exhibits biphasic behaviour, i.e. there exists $t_1 > 0$ such that the per capita growth rate, $\sigma(N(t))$, has the following behaviour:

$$\frac{d\sigma}{dN} \begin{cases} > 0 \text{ for } t \in [0, t_1], \\ < 0 \text{ for } t \in [t_1, T]. \end{cases}$$

Theorem 3 *Necessary and sufficient conditions for the age-structured model with resource-regulated proliferation, Eqs.* (1)–(5), *to exhibit the behaviour B1 and B2 are as follows*

$$\mu < \tau_p^{-1}, \tag{19}$$

$$(\tau_p^{-1} - \mu)Y(t) > \mu X(t) \quad \forall t \in [0, T], \tag{20}$$

and there exists $t_1 > 0$ *such that*

$$\frac{\mathrm{d}}{\mathrm{d}t}\left[\frac{Y}{N}\right] > 0 \, for \, t \in [0, t_1] \quad and \quad \frac{\mathrm{d}}{\mathrm{d}t}\left[\frac{Y}{N}\right] < 0 \, for \, t \in [t_1, T]. \tag{21}$$

Proof Given the relationship in Eq. (17), it is clear that (20) is true if and only if the derivative of N is positive. To derive (21), we notice from the chain rule that $\frac{\mathrm{d}\sigma(N(t))}{\mathrm{d}t} = \frac{\mathrm{d}\sigma(N)}{\mathrm{d}N}\frac{\mathrm{d}N}{\mathrm{d}t}$ and given that $\frac{\mathrm{d}N}{\mathrm{d}t} > 0$, the sign of $\frac{\mathrm{d}}{\mathrm{d}t}(\sigma(N(t)))$ is the same as that of $\frac{\mathrm{d}\sigma(N)}{\mathrm{d}N}$. Finally, condition (19) needs to be satisfied so that the age-structured model has a stable steady-state solution as described in de la Cruz et al. (2016). □

Theorem 3 gives necessary and sufficient conditions for the model to exhibit the behaviour described in B1 and B2. We note that the conditions for the biphasic behaviour are given by Eq. (21) which can be interpreted biologically as an initial increase in the fraction of mature cells followed by a stabilisation phase in which the mature cell fraction decreases to its steady-state value. Since the fraction of mature cells is regulated by the transition age, $a_{G1/S}$, and this critical age is regulated by the resource concentration, we deduce that changes in the resource dynamics may influence the biphasic behaviour.

4 Numerical Results

In this section, we perform numerical simulations to verify the predictions of Theorem 3. First, we present the discretisation scheme that we use to solve Eqs. (1)–(5).

4.1 Discretisation Scheme

The model is composed of a hyperbolic partial differential equation with a nonlocal boundary condition coupled to an ordinary differential equation. We use a splitting method to discretise the coupled system. The ordinary differential equation is discretised by an implicit Euler method. The partial differential equation is discretised using the Rothe method: first discretised in time via the implicit Euler method and then in space by linear finite elements (Grossmann et al. 2007). The method is stabilised by considering the streamline upwind/Petrov Galerkin formulation (Kuzmin 2010). The finite element discretisation is implemented in C++ using the software DEAL.II (Bangerth et al. 2007).

To discretise the age domain $[0, \infty]$, we notice that the cell age is naturally bounded. Hence, there exists $a_{\max} > 0$ such that $n(a, t) = 0$ for $a \in (a_{\max}, \infty)$, and so

we restrict our attention to $a \in [0, a_{\max}]$. For the finite element discretisation to be computationally efficient and not create spurious oscillations around the discontinuity point of the proliferation rate (given by the Heaviside function), we discretise the age domain $[0, a_{\max}]$ differently in two subdomains: the subdomain $[0, a^*]$, where a^* is given by Eq. (8), is discretised with a step size of $h_a = a^*/2^{10} \approx 0.00469081$, and the domain $[a^*, a_{\max}]$ is discretised with a step size of $h_a = (100 - a^*)/2^{10} \approx 0.0442$. We consider a smaller step size for the first domain since for the simulations considered in this work, the evolution of $a_{G1/S}(t)$ occurs in this subdomain. For the time discretisation, we consider a time step of $h_t = 0.1$.

4.2 Model Parametrisation

We consider as a case study, PC-3 prostate cancer cells. In order to parametrise our model, we use as a guideline the parameters that were estimated in Jin et al. (2018) from the experimental time-course data of scratch assays. The authors estimated a proliferation rate of $\hat{\lambda} = 0.053 \pm 0.005 \,(\text{h})^{-1}$. We assume their estimate corresponds in our model to τ_p^{-1}, i.e.

$$\tau_p^{-1} = 0.053 \,(\text{h})^{-1}. \tag{22}$$

Estimates of doubling times of PC-3 prostate cancer cells are in the range of 25–33 h (Bairoch 2018; Cunningham and You 2015). In our model, the doubling time, which we denote as DT, is given by

$$\text{DT} := a_{G1/S}(t) + \tau_p,$$

therefore,

$$25 \leq \text{DT} \leq 33. \tag{23}$$

When the cell population reaches the steady-state age distribution, DT is given by:

$$\text{DT} := a^* + \tau_p = -\frac{1}{\mu} \log\left(\frac{\tau_p(\mu + \tau_p^{-1})}{2}\right) + \tau_p. \tag{24}$$

By considering this formula, the estimated value for the proliferation rate τ_p^{-1} [Eq. (22)] and the range of values for the doubling time [Eq. (23)], we obtain a range of values for the death term, $\mu \in [0.0233 - 0.0333]$. We assume that $\mu = 0.0283 \,(\text{h})^{-1}$ (the midpoint value).

The carrying capacity was also estimated in Jin et al. (2018) they found $\bar{K} = 2.3 \times 10^{-3} \pm 2 \times 10^{-4} \,(\text{cells})/(\mu\text{m})^2$. Since the size of the subregion where they estimated $\bar{K}$ is $1430 \times 200 \,(\mu\text{m})^2$, the carrying capacity in cell number is

$$N_\infty = 657.8 \pm 57.2 \,(\text{cells}). \tag{25}$$

We therefore assume that

$$N_\infty = 657.8 \text{ (cells)}. \tag{26}$$

The oxygen consumption rate of PC-3 prostate cancer cells was measured in Cook et al. (2013) and found to be approximately $\frac{2\,(\text{nM})}{(\text{min})(10^6\text{cells})} = 1.2 \times 10^{-4} \frac{(\text{nM})}{(\text{h})\,(\text{cell})}$. Using this value for the consumption rate, k, and the estimate of the carrying capacity [Eq. (26)] in the formula of the steady-state value of the total population in our model [Eq. (10)], we determine the value of the resource flux, $\bar{S} = 26.63 \times 10^{-4} \frac{(\text{nM})}{(\text{h})}$.

Regarding the parameters that describe the resource dependence of the $G1/S$ transition age, we take the parameter values that were derived from an intracellular model for an oxygen-regulated proliferation rate in de la Cruz et al. (2016), namely, the dimensionless parameter values $\beta = 0.2$ and $c_{\text{cr}} = 0.23$. For determining the parameter value of a_-, we notice that the admissible range of values for $a_{G1/S}(t)$ is $6 \leq a_{G1/S}(t) \leq 14$ given the range values of DT [Eq. (23)] and the estimate of τ_p [Eq. (22)]. We consider $a_- = 8.25$ (h), so $a_{G1/S}(t)$ is in this range for all our simulations.

We consider the following initial age distribution that is a multiple of the steady-state age distribution:

$$v_0(a) = \begin{cases} \kappa \exp(-\mu a) & \text{if } a < a^* \\ \kappa \exp(-\mu a - \tau_p^{-1}(a - a^*)) & \text{if } a \geq a^* \end{cases}$$

where a^* is the steady-state value of the transition age [Eq. (8)] and κ is estimated so the initial number of cells corresponds to the average number of cells considered as initial condition in Jin et al. (2018) for the most confluent initial condition, $N(0) = 223$. We set $c_0 = c_\infty$ as the steady-state value of the resource concentration given by Eq. (9). The default parameters are listed in Table 1.

Table 1 Summary of model parameters

Parameter	Description	Value	Units	References
τ_p^{-1}	Proliferation rate	0.053	$(\text{h})^{-1}$	Jin et al. (2017)
μ	Death rate	0.028	$(\text{h})^{-1}$	Estimated
k	Consumption rate	1.2×10^{-4}	$(\text{h})^{-1}$	Cook et al. (2013)
$\bar{S}$	Resource flux	26.635×10^{-4}	$\frac{(\text{nM})}{(\text{h})}$	Estimated
c_{cr}	Critical resource value	0.023	(nM)	de la Cruz et al. (2016)
β	Scaling constant	0.2	Dimensionless	de la Cruz et al. (2016)
a_-	Scaling constant	8.25	(h)	Assumed
c_0	Initial resource value	0.034	Dimensionless	Estimated
κ	Scaling constant	12.488	Dimensionless	Estimated
a_{max}	Maximum age	100	(h)	Estimated

4.3 Reference Dynamics

Under the default parameter values, the model satisfies the conditions of Theorem 3 and therefore we expect a logistic-type behaviour and a biphasic dynamics. In Fig. 2a, b, we plot the time evolution of the total cell population $N(t)$ and of the resource concentration $c(t)$, respectively. As expected, the total cell population follows a logistic-type behaviour: it grows exponentially and then saturates. The resource concentration has an initial increase until it reaches a maximum value and then decreases until it reaches its steady-state value. In Fig. 2c, we plot the evolution of the transition age $a_{G1/S}$ and observe its dependence on the resource concentration: it decreases to a minimum value and then increases towards the steady-state value given by Eq. (8). In Fig. 2d, we plot the per capita growth rate $\sigma(N)$ as a function of the total cell population N; as expected, we observe biphasic behaviour, with an initial increase in σ with respect to cell density followed by a linear decrease.
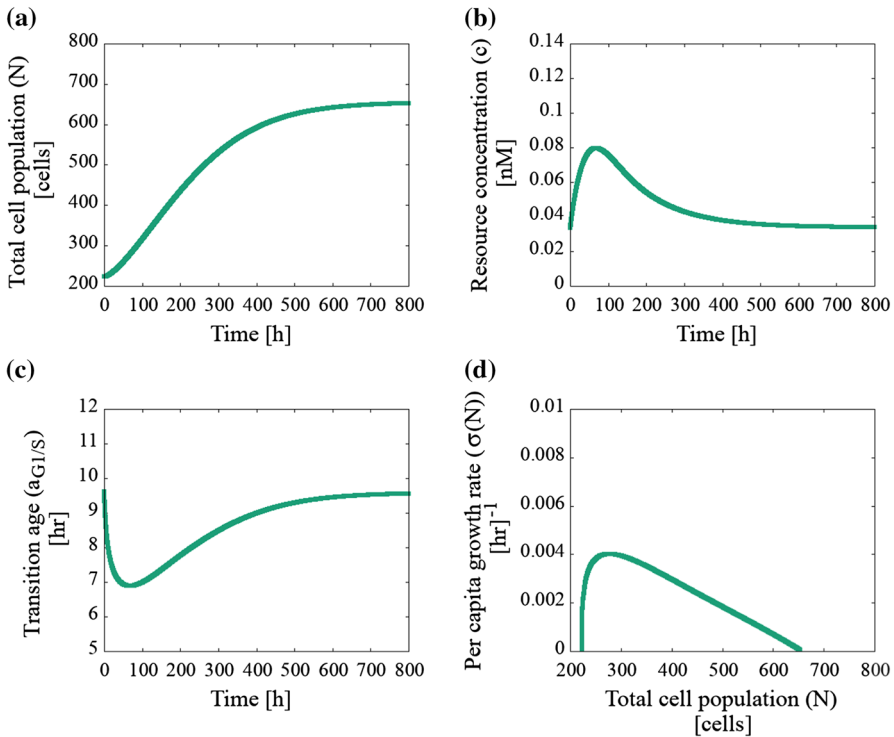
Fig. 2 Evolution of the age-structured model with resource-regulated proliferation, Eqs. (1) and (4). In **a**, we plot the total cell population evolution and observe it follows a logistic-type growth. In **b**, we plot the resource evolution that follows a rapid increase and then a monotonic decrease to the steady-state value. In **c**, we plot the evolution of the transition age $a_{G1/S}(t)$ and the inverse dependence of the resource concentration on the transition age can be observed. In **d**, we plot the per capita growth rate against the total cell population evolution for which two proliferation phases can be observed (a rapid increase, then slower decrease). Parameter values as per Table 1 (Colour figure online)

4.4 Sensitivity Analysis

In this subsection, we perform a sensitivity analysis focusing on those parameters that modulate the resource dynamics in order to understand their role in determining the biphasic behaviour of the per capita growth rate.

We focus our sensitivity analysis on two parameters that can be experimentally manipulated: the resource flux, $\overline{S}$, and the initial concentration of resource, c_0. We first vary the resource flux, $\overline{S}$, in the domain $[25.63 \times 10^{-4} - 28.63 \times 10^{-4}]$. We consider this domain so the cell population steady-state value, N_∞, is within the confidence interval given by Eq. (25). As expected, from Eq. (10), the steady-state value at which the total cell population saturates, N_∞, increases as the value of $\overline{S}$ increases (Fig. 3). We observe also that the maximum value of $c(t)$ increases and the minimum value of $a_{G1/S}(t)$ decreases as $\overline{S}$ increases, see Fig. 3c, d. We observe in Fig. 3d that the biphasic behaviour is present for all values of the resource flux that were considered.

We now vary the initial resource concentration c_0. We focus only on increasing the value of the resource concentration above c_∞, since considering values below c_∞

(a)

(b)

(c)

$\overline{S}= 25.63 \times 10^{-4}$
$\overline{S}= 26.63 \times 10^{-4}$
$\overline{S}= 24.63 \times 10^{-4}$
$\overline{S}= 27.63 \times 10^{-4}$
$\overline{S}= 28.63 \times 10^{-4}$

(d)
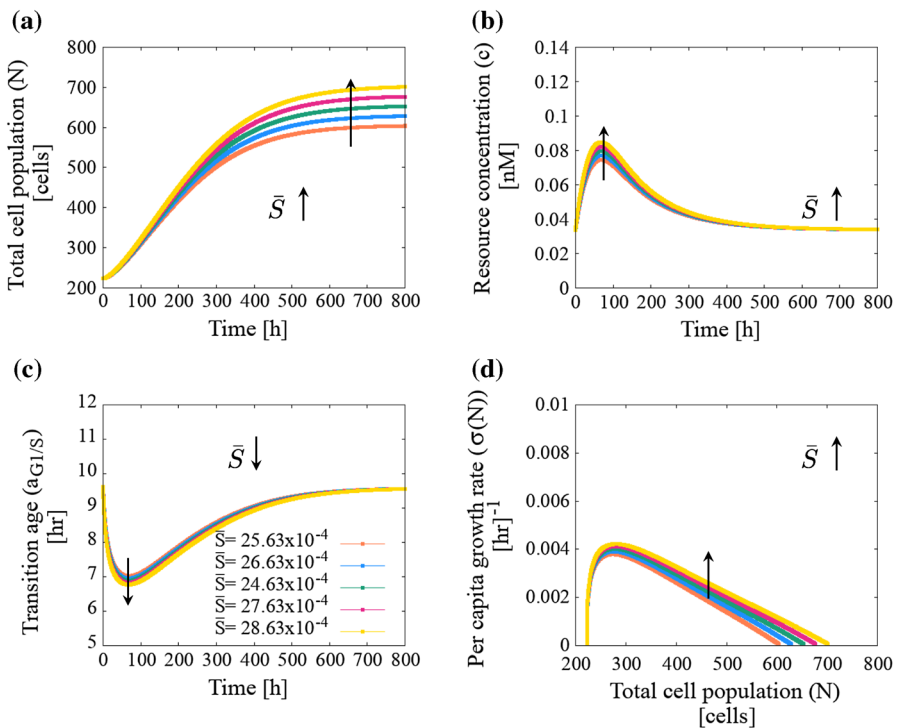
Fig. 3 Series of plots showing the dynamics of the coupled age-structured model with resource-regulated proliferation given by Eqs. (1) and (4), as we vary the resource flux, $\overline{S}$. Increasing the value of $\overline{S}$: **a** increases the steady-state value of the total cell population, N_∞, **b** increases the maximum resource concentration and the time it takes to reach the steady-state value, and **c** reduces the minimum value of the transition age $a_{G1/S}$. **d** The plots of the per capita growth rate against the total cell population exhibit biphasic dynamics for the selected values of $\overline{S}$. Parameter values as per Table 1 (Colour figure online)

(a)

(b)

(c)

(d)
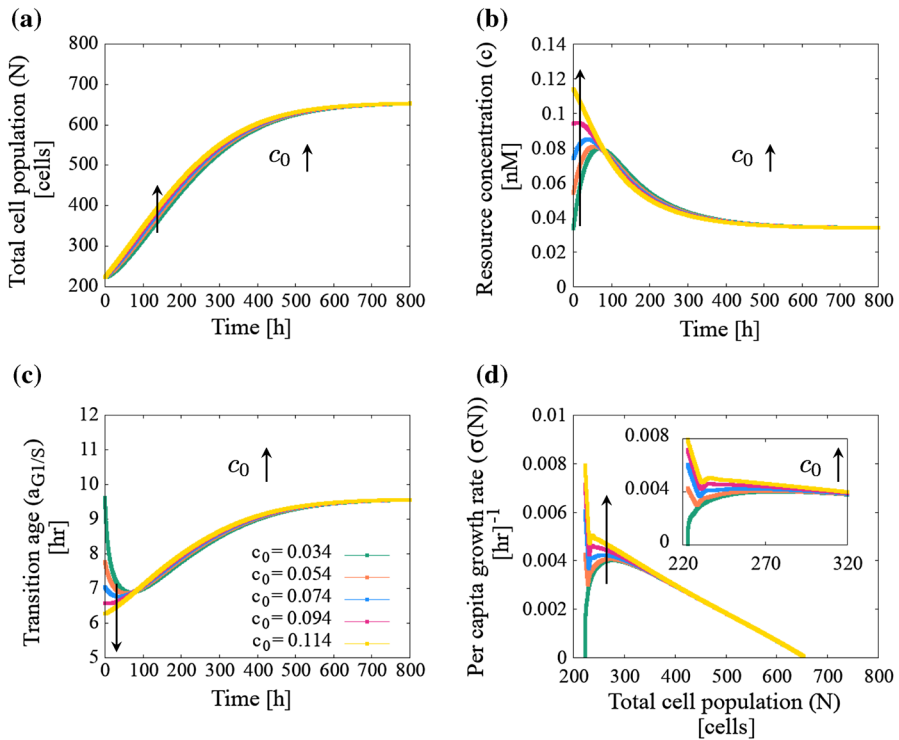
Fig. 4 Series of plots showing the dynamics of the coupled age-structured model with resource-regulated proliferation, given by Eqs. (1) and (4), as we vary the initial resource concentration value, c_0. Increasing c_0: **a** does not affect the total cell population, **b** increases the maximum resource concentration but reduces the time it takes to reach it, and **c** makes the initial decrease of the transition age $a_{G1/S}$ disappear. **d** Increasing the initial resource concentration, c_0, affects the plots of the per capita growth rate against the total cell population by shortening the duration of the disturbance phase where there is no monotonic decreasing dependence. Parameter values as per Table 1 (Colour figure online)

will make the population decrease and this will be in disagreement with experimental observations. In Fig. 4, we show that when we increase c_0, from 0.034 to 0.114, the duration of the disturbance phase is shortened. The model predicts that by increasing c_0, the total cell population evolution does not change significantly; however, the resource evolution changes from biphasic to monotonic, i.e. the duration of the disturbance phase decreases and eventually disappears as c_0 increases (see Fig. 4b). Increasing the value of the initial resource concentration shifts the observation time of the dynamics and now it is only possible to observe the resource concentration decline to the steady-state value. This effect can be similarly observed in Fig. 4c where the initial decrease of the transition age $a_{G1/S}$ is shortened as c_0 increases. We observe that increasing the initial resource concentration decreases the duration of the disturbance phase where the dependence of the per capita growth rate with respect to the total cell population is not linear (see Fig. 4d). We notice that during the disturbance phase, the per capita growth rate does not increase monotonically with respect to the total cell population as we saw previously for the reference dynamics and when varying the

resource flux, $\overline{S}$. For the simulations with c_0 bigger than $c_\infty = 0.034$, the per capita growth rate initially decreases, then increases and finally follows a linear decreasing trend with respect to the total cell population.

Finally, we perform a sensitivity analysis on the rest of the model parameters and consider different initial age distributions to show that our model predictions are robust. We observe that uncertainty in the parameter values over the range of values that we considered, has little effect on the overall dynamics. The two proliferation phases are present for all the sets of parameters considered (see Supporting Information Sect. 1). We then consider different initial age distributions that satisfy the conditions of Theorem 3 and show that the biphasic dynamics is present in all cases considered (see Supporting Information Sect. 2). We also analyse the model behaviour when the resource concentration is below the critical value, $c(t) < c_{cr}$. We show that in this situation the population initially decreases and the per capita growth rate is constant (see Supporting Information Sect. 3).

5 Discussion and Conclusions

In this work, we have presented an age-structured model with resource-dependent proliferation rate that captures for the first time the biphasic behaviour in the per capita growth observed experimentally in Jin et al. (2017). We analysed the full model in terms of two subpopulations: cells which are able to proliferate or not (mature and immature cells). We then derived necessary and sufficient conditions under which the model presents a logistic-type behaviour and two phases of proliferation: an initial phase, which in Jin et al. (2017) was named *disturbance phase,* in which proliferation does not follow a logistic growth, and a *growth phase,* where proliferation is approximately logistic. The biphasic behaviour was demonstrated to be a result of an initial increase of the fraction of mature cells followed by a decline to their steady-state concentration. We then parametrised the model using PC-3 prostate cancer cells as a case study. Finally, through numerical simulations, we showed that varying the resource initial value results in a change in the dependence of the per capita growth rate on the total cell population. The model predicts that the duration of the disturbance phase is decreased as the initial resource concentration is increased.

In view of this model, the experimental observations in Jin et al. (2017) can be explained as follows: the scratch procedure decreases the cell number in the plate and by replenishing the medium to the same quantity, as customary, the resource concentration is increased, therefore triggering the biphasic dynamics in the per capita growth rate. The predictions of the model could be experimentally tested by modifying the resource concentration in the substrate, examining the plots of per capita growth rate against the total cell population, as was performed in Jin et al. (2017), and measuring the resource concentration, as in Billy et al. (2012), at the same times as the cell population density is captured. The model predicts that by increasing the initial resource concentration, the disturbance phase would shorten. Varying the resource concentration has been shown to affect the overall dynamics of the scratch assay in other situations (Billy et al. 2012).

The age-structured model has some limitations. There is a critical constraint in the biologically realistic parameter regime. The parameters need to be chosen such that $\frac{da_{G1/s}(t)}{dt} < 1$ for all $t \in [0, T]$. Otherwise, cells could go from the S–G2–M phase back to the G1 phase without proliferating [see Eq. (12)]. In all our simulations, the derivative of the transition age is always less than one (results not shown). To avoid restricting the parameter regime, age-structured models with multiple compartments for the cell cycle phases (Billy et al. 2012; Chaffey et al. 2014) can be considered.

There are different ways that we can extend this work. The model was parametrised using estimates calculated in Jin et al. (2017). Their estimates were calculated with respect to the logistic equation and since we are considering a different model, the values are expected to differ. The model could be parametrised using more appropriate methods as has been done for similar models (Gabriel et al. 2012; Billy et al. 2012). We acknowledge that our age-structured model is just one of many possible explanations for the biphasic behaviour observed experimentally in Jin et al. (2017). Mechanical and chemical disturbances have been known to affect cell proliferation in other experimental settings (Nyegaard et al. 2016). Models that integrate explicitly biochemical pathways, such as those in Domschke et al. (2017) and Nardini and Bortz (2018), can be adapted to investigate whether the biphasic behaviour is a product of signalling events. An inference-based modelling approach could be performed to test multiple hypotheses and assist with the design of experiments that discriminate between feasible alternatives.

In summary, this work identifies the interplay between the mature subpopulation and the resource concentration as a plausible explanation for the biphasic behaviour observed experimentally in Jin et al. (2017). Experimental validation and further mathematical modelling will help elucidate the impact of heterogeneity in cell age distribution in the overall dynamics.

References

Adan A, Kiraz Y, Baran Y (2016) Cell proliferation and cytotoxicity assays. Curr Pharm Biotechnol 17(14):1213–1221

Bairoch A (2018) The cellosaurus, a cell-line knowledge resource. J Biomol Tech JBT 29(3):25–38

Baker RE, Simpson MJ (2010) Correcting mean-field approximations for birth-death-movement processes. Phys Rev E 82(4):041905

Bangerth W, Hartmann R, Kanschat G (2007) deal. IIa general-purpose object-oriented finite element library. ACM Trans Math Softw (TOMS) 33(4):24

Billy F, Clairambault J (2013) Designing proliferating cell population models with functional targets for control by anti-cancer drugs. Discrete Cont Dyn Syst Ser B 18(4):865–889

Billy F, Clairambault J, Delaunay F, Feillet C, Robert N (2012) Age-structured cell population model to study the influence of growth factors on cell cycle dynamics. Math Biosci Eng 10(1):1–17

Bourseguin J, Bonet C, Renaud E, Pandiani C, Boncompagni M, Giuliano S, Pawlikowska P, Karmous-Benailly H, Ballotti R, Rosselli F et al (2016) FANCD2 functions as a critical factor downstream of MiTF to maintain the proliferation and survival of melanoma cells. Sci Rep 6:36539

Browning AP, McCue SW, Simpson MJ (2017) A Bayesian computational approach to explore the optimal duration of a cell proliferation assay. Bull Math Biol 79(8):1888–1906

Celis JE (2009) Cell biology assays: essential methods. Butterworth-Heinemann, Oxford

Chaffey GS, Lloyd DJB, Skeldon AC, Kirkby NF (2014) The effect of the G1-S transition checkpoint on an age structured cell cycle model. PLoS ONE 9(1):e83477

Cohen SM, Ellwein LB (1990) Cell proliferation in carcinogenesis. Science 249(4972):1007–1011

Cook CC, Kim A, Terao S, Gotoh A, Higuchi M (2013) Consumption of oxygen: a mitochondrial-generated progression signal of advanced cancer. Cell Death Dis 3(1):e258

Cunningham D, You Z (2015) In vitro and in vivo model systems used in prostate cancer research. J Biol Methods 2(1):e17

Darnell JE, Lodish HF, Baltimore D et al (1990) Molecular cell biology, vol 2. Scientific American Books New York, New York

de la Cruz R, Guerrero P, Spill F, Alarcón T (2016) Stochastic multi-scale models of competition within heterogeneous cellular populations: simulation methods and mean-field analysis. J Theor Biol 407:161–183

Domschke P, Trucu D, Gerisch A, Chaplain MAJ (2017) Structured models of cell migration incorporating molecular binding processes. J Math Biol 75(6–7):1517–1561

Foster DA, Yellen P, Xu L, Saqcena M (2010) Regulation of G1 cell cycle progression: distinguishing the restriction point from a nutrient-sensing cell growth checkpoint (s). Genes Cancer 1(11):1124–1131

Gabriel P, Garbett SP, Quaranta V, Tyson DR, Webb GF (2012) The contribution of age structure to cell population responses to targeted therapeutics. J Theor Biol 311:19–27

Gavagnin E, Ford MJ, Mort RL, Rogers T, Yates CA (2018) The invasion speed of cell migration models with realistic cell cycle time distributions. arXiv:1806.03140

Gerlee P (2013) The model muddle: in search of tumour growth laws. Cancer Res 73(8):2407–2411

Grossmann C, Roos HG, Stynes M (2007) Numerical treatment of partial differential equations, vol 154. Springer, Berlin

Jin W, Shah ET, Penington CJ, McCue SW, Chopin LK, Simpson MJ (2016) Reproducibility of scratch assays is affected by the initial degree of confluence: experiments, modelling and model selection. J Theor Biol 390:136–145

Jin W, Shah ET, Penington CJ, McCue SW, Maini PK, Simpson MJ (2017) Logistic proliferation of cells in scratch assays is delayed. Bull Math Biol 79(5):1028–1050

Jin W, McCue SW, Simpson MJ (2018) Extended logistic growth model for heterogeneous populations. J Theor Biol 445:51–61

Johnston ST, Shah ET, Chopin LK, McElwain DS, Simpson MJ (2015) Estimating cell diffusivity and cell proliferation rate by interpreting IncuCyte ZOOM assay data using the Fisher–Kolmogorov model. BMC Syst Biol 9(1):38

Kermack WO, McKendrick AG (1932) Contributions to the mathematical theory of epidemics. II. The problem of endemicity. Proc R Soc Lond A 138(834):55–83

Keyfitz BL, Keyfitz N (1997) The McKendrick partial differential equation and its uses in epidemiology and population study. Math Comput Modell 26(6):1–9

Kramer N, Walzl A, Unger C, Rosner M, Krupitza G, Hengstschläger M, Dolznig H (2013) In vitro cell migration and invasion assays. Mutat Res Rev Mutat Res 752(1):10–24

Kuzmin D (2010) A guide to numerical methods for transport equations. University Erlangen-Nuremberg, Erlangen

Liang CC, Park AY, Guan JL (2007) In vitro scratch assay: a convenient and inexpensive method for analysis of cell migration in vitro. Nat Protoc 2(2):329

Lim S, Kaldis P (2013) Cdks, cyclins and CKIs: roles beyond cell cycle regulation. Development 140(15):3079–3093

Liu JC, Zacksenhouse M, Eisen A, Nofech-Mozes S, Zacksenhaus E (2017) Identification of cell proliferation, immune response and cell migration as critical pathways in a prognostic signature for HER2+: ERα-breast cancer. PLoS ONE 12(6):e0179223

Maini PK, McElwain DS, Leavesley D (2004) Travelling waves in a wound healing assay. Appl Math Lett 17(5):575–580

Masuzzo P, Van Troys M, Ampe C, Martens L (2016) Taking aim at moving targets in computational cell migration. Trends Cell Biol 26(2):88–110

Menyhárt O, Harami-Papp H, Sukumar S, Schäfer R, Magnani L, de Barrios O, Győrffy B (2016) Guidelines for the selection of functional assays to evaluate the hallmarks of cancer. Biochim Biophys Acta (BBA) Rev Cancer 1866(2):300–319

Nardini JT, Bortz DM (2018) Investigation of a structured Fisher's equation with applications in biochemistry. SIAM J Appl Math 78(3):1712–1736

Nyegaard S, Christensen B, Rasmussen JT (2016) An optimized method for accurate quantification of cell migration using human small intestine cells. Metab Eng Commun 3:76–83

Ortmann B, Druker J, Rocha S (2014) Cell cycle progression in response to oxygen levels. Cell Mol Life Sci 71(18):3569–3582

Romar GA, Kupper TS, Divito SJ (2016) Research techniques made simple: techniques to assess cell proliferation. J Investig Dermatol 136(1):e1–e7

Sarapata EA, de Pillis L (2014) A comparison and catalog of intrinsic tumor growth models. Bull Math Biol 76(8):2010–2024

Savla U, Olson LE, Waters CM (2004) Mathematical modeling of airway epithelial wound closure during cyclic mechanical strain. J Appl Physiol 96(2):566–574

Smith J, Winslow D, Rudland P (1984) Different growth factors stimulate cell division of rat mammary epithelial, myoepithelial, and stromal cell lines in culture. J Cell Physiol 119(3):320–326

Topman G, Sharabani-Yosef O, Gefen A (2012) A standardized objective method for continuously measuring the kinematics of cultures covering a mechanically damaged site. Med Eng Phys 34(2):225–232

Vittadello ST, McCue SW, Gunasingh G, Haass NK, Simpson MJ (2018) Mathematical models for cell migration with real-time cell cycle dynamics. Biophys J 114(5):1241–1253

Walker D, Hill G, Wood S, Smallwood R, Southgate J (2004a) Agent-based computational modeling of wounded epithelial cell monolayers. IEEE Trans Nanobiosci 3(3):153–163

Walker D, Southgate J, Hill G, Holcombe M, Hose D, Wood S, Mac Neil S, Smallwood R (2004b) The epitheliome: agent-based modelling of the social behaviour of cells. Biosystems 76(1–3):89–100

Warne D, Baker R, Simpson M (2018) Using experimental data and information criteria to guide model selection for reaction-diffusion problems in mathematical biology. Bull Math Biol 81(6):1–45

West GB, Brown JH, Enquist BJ (2001) A general model for ontogenetic growth. Nature 413(6856):628

Affiliations

Ana Victoria Ponce Bobadilla[1,2] (ID) · **Thomas Carraro**[1,2] (ID) · **Helen M. Byrne**[3] (ID) · **Philip K. Maini**[3] (ID) · **Tomás Alarcón**[4,5,6,7] (ID)

1   Institute for Applied Mathematics, Heidelberg University, 69120 Heidelberg, Germany

2   Interdisciplinary Center for Scientific Computing (IWR), Heidelberg University, 69120 Heidelberg, Germany

3   Wolfson Centre for Mathematical Biology, Mathematical Institute, University of Oxford, Oxford OX2 6GG, UK

4   ICREA, Pg. Lluís Companys 23, 08010 Barcelona, Spain

5   Centre de Recerca Matemàtica, Edifici C, Campus de Bellaterra, 08193 Bellaterra, Barcelona, Spain

6   Barcelona Graduate School of Mathematics (BGSMath), Barcelona, Spain

7   Departament de Matemàtiques, Universitat Autònoma de Barcelona, 08193 Bellaterra, Barcelona, Spain